

## Picosecond Self-Induced Thermal Lensing from Colloidal Silver Nanodisks

Mathieu Maillard<sup>†</sup> and Marie-Paule Pileni\*

Laboratoire des Matériaux Mesoscopiques et Nanométriques, BP 52, Université Pierre et Marie Curie, 4 Place Jussieu, 75005 Paris, France

Stephan Link<sup>‡</sup> and Mostafa A. El-Sayed\*

Laser Dynamics Laboratory, School of Chemistry and Biochemistry, Georgia Institute of Technology, 770 State Street, Atlanta, Georgia 30332-0400

Received: January 6, 2004; In Final Form: February 20, 2004

The optical and nonradiative relaxation dynamics of 5 nm thick silver nanodisks with a 25 nm diameter have been investigated in an organic solvent by continuous wave (cw) and femtosecond pump–probe time-resolved spectroscopies. Several surface plasmon absorption bands are observed due to the disk shape of these particles. In the time-resolved experiments, the time dependence of the bleach resulting from femtosecond pulsed excitation is studied. On the 1–3 ps time scale, a decay resulting from electron–phonon relaxation is observed. On a longer time scale (>20 ps), a rise rather than a further decay of the bleach intensity is observed. This is shown to result from the formation of a thermal lens due to the induced thermal gradients produced from heating the organic solvent by the phonon–phonon relaxation processes of the photoexcited nanodisks.

### Introduction

Research concerning nanomaterials is at the interface of a variety of scientific domains as different as materials chemistry, quantum physics or optical physics. Shape controlled nanoparticle synthesis is of great interest for numerous groups because it is important in understanding and controlling their particular physical properties. This has been carried out for a wide variety of particle shapes such as spheres,<sup>1</sup> nanorods,<sup>2</sup> cubes,<sup>3</sup> or triangles.<sup>4</sup> A wide variety of physical methods have been developed to characterize them and determine their properties as a function of shape. In the field of time-resolved spectroscopy, the nanoparticle electronic confinement as well as electron–phonon coupling or thermal and acoustic relaxation have been studied.<sup>5–8</sup> Most of the time-resolved studies have focused on the size and shape dependence of the electron–phonon relaxation trying to understand how the electron–phonon coupling changes when the size of the particles is reduced. Recently, the question of thermal energy transfer between the excited nanoparticles and the surrounding medium was addressed in several studies.<sup>9–12</sup> Thermal equilibration between the lattice and the surrounding medium becomes especially important for higher laser excitation powers. In the case of gold nanorods,<sup>13</sup> using higher excitation densities, a shape transformation of the gold nanorods in aqueous solution into spherical particles was observed. The time scales involved and the efficiencies of the laser-induced shape transformation should be highly influenced by the thermal heat loss of the particles following excitation. The cooling dynamics of the lattice is therefore an important but also much less understood part of the electron dynamics in small nanoparticles. In fact, it has been pointed out that<sup>10–12</sup>

the rate of phonon–phonon relaxation processes that cool off the nanoparticles could be limited by the heat diffusion away from the surrounding medium (through the capping material and immediate surrounding solvent). In this case, the long decay time would be a measure of the surrounding solvent cooling, which then controls the overall rate of the nanoparticle cooling.

In the present work, we present a time-resolved study of the thermal relaxation dynamics of disk-shaped silver nanoparticles encapsulated in micelles using femtosecond pulse excitation. Silver disk-shaped particles have been synthesized by a new chemical method that enables one to synthesize particles differing in their size at constant aspect ratio.<sup>14,15</sup> The disk shape induces a large modification of the optical properties by splitting the plasmon resonance. By probing the bleach recovery of the surface plasmon resonance after laser excitation, we can follow the electron–phonon relaxation of an excited metal nanoparticle, which is on the order of a few picoseconds. After the initial bleach recovery we observe, however, an increase in the bleach intensity on a much longer time scale (>20 ps). We attribute this effect to the creation of a thermal lens induced by the heat transfer from the hot nanoparticles to the surrounding medium. This gives additional information on the energy transfer processes involved between the particles and the medium.

The thermal lens effect has widely been used to probe the nonradiative relaxation of excited states in molecules.<sup>16,17</sup> In analogy, the cooling of the excited metal nanoparticles also involves nonradiative heat loss, which can be followed by thermal lens spectroscopy. Recently, imaging using the thermal lens effect has been demonstrated as an important new method because it allows the imaging of subwavelength objects with a far field technique.<sup>18,19</sup>

### Experimental Section

**Silver Nanodisks Synthesis.** Silver bis(2-ethylhexyl)sulfosuccinate, Ag(AOT), is made as described previously.<sup>20</sup> Col-

\* Corresponding authors. E-mail: M.P.P., pileni@sri.jussieu.fr; M.A.E., mostafa.el-sayed@chemistry.gatech.edu.

<sup>†</sup> Current address: Department of Chemistry, Columbia University, 3000 Broadway, New York, NY 10027.

<sup>‡</sup> Current address: School of Chemistry and Biochemistry, University of Texas at Austin, Austin, TX 78712.

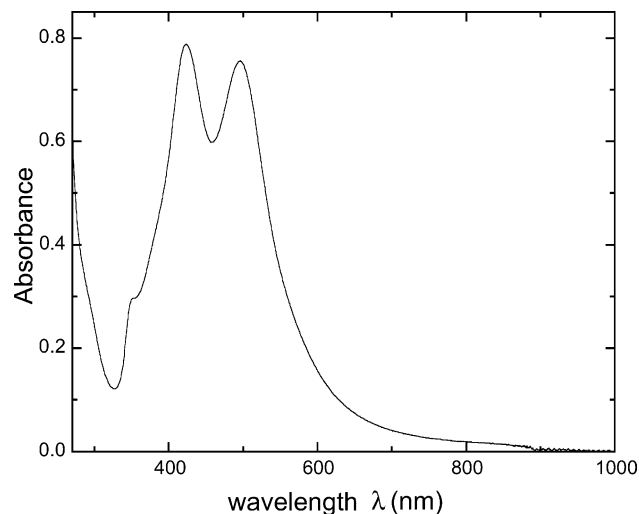


**Figure 1.** Continuous wave (cw) absorption spectrum of a solution of silver nanodisks. The strong band at 420 nm is due to spheres whereas the shoulder at 350 nm and the strong band at 500 nm are due to the transverse and longitudinal surface plasmon resonance of the nanodisks having a diameter of 25 nm with a thickness of 5 nm.

loidal silver particles are obtained by mixing two solutions.<sup>14</sup> The first one is a reverse micelle solution made of 60% 0.1 M Ag(AOT) and 40% 0.1 M Na(AOT) solubilized in isoctane. The water molar ratio,  $w = [\text{H}_2\text{O}]/[\text{AOT}]$ , is kept at 2. The second one is 0.1 M Na(AOT) in isoctane, with water replaced by hydrazine ( $\text{N}_2\text{H}_4$ ). The overall hydrazine concentration varies from 0.5 to 1.66 M and the molar ratio  $y = [\text{N}_2\text{H}_4]/[\text{AOT}]$ , is changed from 5 to 16.6. After the hydrazine is added, the solution is stirred for 20 min and becomes opalescent because of a phase transition as the reverse micelles are no longer formed. The two solutions are then mixed together and a dark color quickly appears. The solution is then diluted 100 times in 0.1 M Na(AOT) solution and ultrasonicated for 10 min. Dodecanethiol is then added (20  $\mu\text{L}/\text{mL}$ ). After 2 h the solution is centrifuged, the supernatant solution is removed and the particles are dispersed in a 0.1 M Na(AOT) solution in isoctane.

**Time-Resolved Experiments.** Transient absorption studies<sup>11</sup> were performed using an amplified Ti:Sapphire laser system (Clark CPA 1000). The second harmonic of the 800 nm fundamental was used as excitation and a white light continuum probe beam was generated by focusing a small part of the fundamental beam into a sapphire window. The beam was split into two parts and used for signal and reference. The signal beam is overlapped with the pump beam after focusing and is then collected behind the sample and focused onto the entrance of a fiber optic cable connected to the monochromator/spectrograph. The pump beam was mechanically chopped and the differential transmission signal was recorded using a pair of Si photodiodes (Thorlab) and a lock-in amplifier (Stanford Research Systems). For spectral measurements a liquid nitrogen cooled CCD camera (Princeton Instruments) in combination with a spectrograph were used.

## Results and Discussion

The synthesis of silver nanodisks described above produces a mixture of disk-shaped particles as well as spheres as impurities. As observed by a transmission electron microscope (TEM), spherical particles have been estimated as 30% in volume. The absorption spectrum of a solution containing disks and spheres is shown in Figure 1 and exhibits mainly three absorption bands attributed to the surface plasmon resonance

from the spheres and nanodisks.<sup>14</sup> The absorption band centered at 420 nm is mainly due to the spheres. Similar to gold nanorods for which the surface plasmon resonance splits into two modes,<sup>8</sup> the surface plasmon resonance for silver nanodisks also strongly depends on the particle shape and size. The high-energy plasmon resonance of the silver disks, located at 350 nm, corresponds to the nanodisk transverse plasmon mode. The low-energy one, located at 500 nm, is attributed to the nanodisk longitudinal surface plasmon resonance.

Isoctane solutions of nanodisks are studied by femtosecond time-resolved pump-probe spectroscopy. The wavelength of the pump is 400 nm whereas the probe can be tuned between 450 and 700 nm using a white light continuum to probe the entire spectrum of the nanodisks. For the dynamics studies, the wavelength of the probe was set to coincide with the longitudinal nanodisk surface plasmon absorption. After femtosecond laser excitation ( $\sim 100$  fs), the particle electronic temperature is increased above that of the lattice of the particles. It has been shown for spherical silver particles<sup>5</sup> that the surface plasmon resonance is red shifted and broadened at higher electronic temperatures. For this reason, if the probe wavelength is below the plasmon resonance, it can be observed as a transient bleach. Conversely, above the plasmon resonance, it can be observed as an increase in absorption. The transient absorption spectrum of silver nanodisks after 400 nm excitation is shown in the inset of Figure 2A. The spectrum was recorded 850 fs after excitation just before a complete temperature equilibrium between the electrons and lattice is reached. The spectrum exhibits the expected bleach and absorption for the longitudinal surface plasmon resonance at 500 nm. The main part of Figure 2A shows the absorption before and 850 fs after excitation whereas the inset is the difference spectrum.

A thermal equilibrium between the initially excited electrons and the lattice is reached as a result of electron-phonon relaxation processes in a few picoseconds for most metal nanoparticles.<sup>5-8</sup> This can be measured by probing the bleach recovery dynamics at 480 nm as a function of delay time between the pump and probe pulses and is shown in Figure 3A. The bleach recovery is dominated by a fast decay component ascribed to the electron-phonon coupling. This fast component can be fitted to an exponential decay  $e^{-t/\tau_{\text{ph}}}$  where  $\tau_{\text{ph}} = 1.8$  ps corresponding to the electron-phonon relaxation time (see Figure 3A). This is comparable to the values observed for the silver and gold spheres as well as rods.<sup>5,8</sup> This confirms the previous conclusion<sup>8</sup> that the electron-phonon relaxation in gold and silver is shape independent for particles larger than about 10 nm.

Thermal relaxation of the particle lattice, which transfers the excitation energy to the surrounding medium, is the final relaxation of the hot metal nanoparticles. Often a second longer decay component of the plasmon band bleach is observed on the few hundred picosecond time scale,<sup>6-8</sup> which has been attributed to the time it takes the heat to exchange between the particle and the surrounding medium and the solvent to reach thermal equilibrium. However, some studies<sup>11,12</sup> suggest that the local energy exchange between the nanoparticles and the solvent molecules surrounding the particles can occur on a similar time scale as the electron-phonon relaxation. The long decay component is thus mainly due to the heat transfer away from the medium immediately surrounding the particle surface. In general, the amplitude of the second component increases with increasing excitation power.<sup>6-8</sup> In the case of the silver nanodisks in isoctane solution, however, a very different behavior is observed at longer delay times. Figure 3B shows

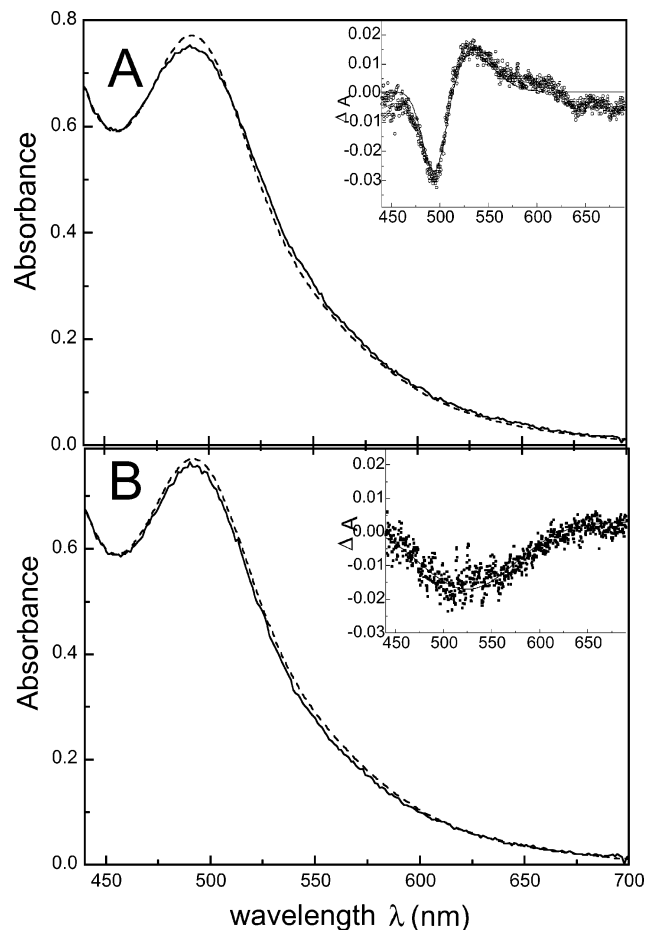


**Figure 2.** Examining the shape of the transient absorption of the nanodisk at different time delays after laser excitation. (A) cw (dashed line) and transient (solid line) absorption spectra of silver nanodisks at a delay time of  $\Delta t = 0.85$  ps and pump energy of  $0.17 \mu\text{J}$  per pulse at 400 nm. The inset shows the difference spectrum. The spectral shape of the transient absorption spectrum is caused by a shift and a broadening of the plasmon resonance due to a higher electron temperature. (B) cw (dashed line) and transient (solid line) absorption spectra of silver nanodisks at a time delay of  $\Delta t = 100$  ps. The pump energy is  $0.17 \mu\text{J}$  per pulse. The inset shows the difference spectrum. In comparison to the early delay time, the spectrum reveals a constant decrease of the absorption intensity but retains its band shape.

the bleach recovery dynamics probed at 480 nm for different excitation energies (see figure legend). Instead of observing a second longer bleach decay component, a rise in the bleach intensity is observed, which increases with increasing delay time as well as with excitation energy. This rise can be fitted to an exponential growth,  $1 - e^{-t/\tau_2}$  with  $\tau_2 = 40$  ps. The intensity of the observed bleach signal can exceed the initial zero-time signal (as seen in Figure 3B). At longer time ( $t > 100$  ps), the signal is found to keep increasing linearly, up to 500 ps, with a slow characteristic time  $\tau_3 = 5.9$  ns.

A similar increase of the plasmon band bleach was previously reported for spherical silver<sup>6</sup> as well as gold<sup>8</sup> nanoparticles. For the silver nanoparticles<sup>6</sup> it was proposed that a temperature increase of the solvent (water) changes the dielectric constant of the surrounding medium, which in turn leads to a blue shift of the plasmon band according to Mie theory.<sup>8</sup> The blue shift causes an increase in the bleach intensity at later delay times as it takes time for the energy exchange with the surrounding medium. To investigate if the signal in our experiment is also due to a shift in the plasmon band, a transient absorption spectrum is recorded at long delay times and compared with

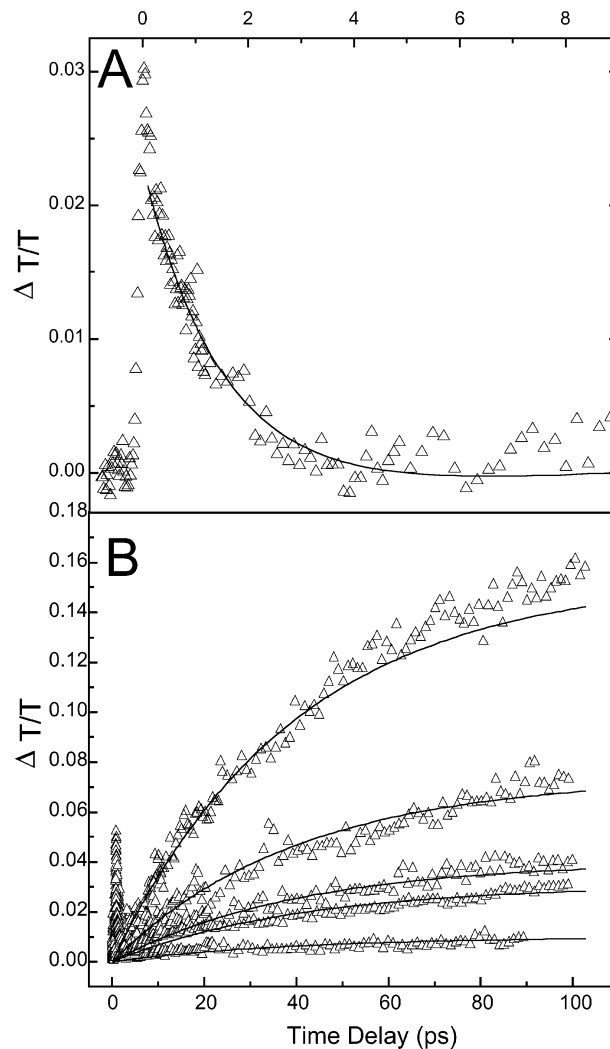


**Figure 3.** (A) Transient absorption dynamics recorded as a function of time delay between 400 nm pump and 480 nm probe pulses. The pump energy is  $0.17 \mu\text{J}$ . The fast decay dynamics can be fitted to a monoexponential decay with a decay time  $\tau_{\text{ph}} = 1.8$  ps. This bleach relaxation corresponds to the thermal equilibration between the electrons and the lattice (electron–phonon relaxation). (B) Transient absorption dynamics recorded for different excitation energies ( $\lambda_{\text{pump}} = 400$  nm;  $\lambda_{\text{probe}} = 480$  nm) and monitored for longer delay times. The pulse energy increases for the traces shown from bottom to top (0.19, 0.26, 0.42, 0.68, and  $1.05 \mu\text{J}$ ). The increase in the bleach intensity at longer delay times is attributed to a thermal lensing effect caused by the rapid heat transfer from the metal nanodisks to the local environment. The data were fit to the sum of an exponential decay and a rise according to  $A + Be^{-t/\tau_1} + C(1 - e^{-t/\tau_2})$  with  $\tau_1 = 1.5$  ps and  $\tau_2 = 40$  ps.

that measured at short delay times. Figure 2B shows that the transient absorption spectrum recorded 100 ps after excitation with 400 nm femtosecond laser pulses compares well with the ground state spectrum of silver nanodisks. The results show that the transient absorption on this time scale does not significantly change its band shape or position. The plasmon resonance decreases in intensity without a noticeable shift or broadening of the plasmon band. A change of the dielectric constant alone due to solvent heating can therefore be ruled out as a possible explanation of the results.

The increase in the bleach intensity could also be attributed to the beginning of a coherent breathing mode of the metal nanoparticles after laser heating, as has been shown for spherical silver and gold nanoparticles.<sup>5,7</sup> However, on the basis of the size of the particles, an oscillation period of about 8 ps is expected. In fact, a steady increase of the bleach intensity up

to 500 ps is observed, which would correspond to a much slower oscillation frequency.

Another possible explanation of the observed behavior is that the concentration of nanoparticles in the excitation volume is decreased due to a volume expansion of the heated area (after the absorbed laser energy has been transferred to the medium). Such an expansion would cause the effective nanoparticle concentration to decrease, which would also mean that the absorption intensity decreases. Taking into account that isooctane has a large thermal relaxation time ( $\tau_{\text{th}} = R^2/\alpha = 6$  ns),<sup>25</sup> thermalization in the nanoparticles surrounding medium is a slow process and such a dilatation effect is unexpected at early time delay in organic solvents. Furthermore, the temperature and volume variation inside the focal volume can be estimated as  $\Delta T = E/mc_p = 0.007$  K and  $\Delta V/V = \beta\Delta T/T = 0.007 \times 10^{-3} = 7 \times 10^{-6}$  for a maximum pulse energy of 1  $\mu\text{J}$ . Hence, volume expansion per pulse is very weak compared to the measured signal and the sample spinning prevents any further increase from the pulse repetition rate. For these reasons, if not negligible, the thermal expansion likely explains the slow rise component at long time delay ( $\Delta t > 100$  ps).

The intermediate exponential behavior ( $5 < t < 100$  ps) is attributed to a thermal lensing effect. Such an effect is often observed in solutions containing strongly absorbing molecules with low fluorescence quantum efficiencies. Thermal lensing spectroscopy<sup>16,21,22</sup> has in fact been used to study radiationless transitions in molecules. After irradiation by light, energy transfer to the solvent occurs by a nonradiative relaxation of the molecular excited state. Taking into account that a laser beam has a Gaussian intensity distribution, molecules are not equally irradiated in the focal volume. Because of that, solvent heating is not spatially homogeneous and temperature gradients are induced in the solvent. As the medium refractive index depends on temperature, a refractive index gradient causes a transient divergent lens to be formed in the excitation volume.

This chromatic aberration has two opposite effects depending on the sample position compared to the beam focal point.<sup>23</sup> If the focal point is in front of the sample, the beam is further dispersed and the signal decreases. On the other hand, if the focal point is behind the sample, the beam converges and the measured signal is increased. In our case, the sample is large compared to the focal volume and the beam is focused inside the sample. According to Lambert–Beer's law, more light is absorbed by particles in the front part of the sample than in the back part. The temperature rise is therefore higher in the front of the sample, and the beam should be converging while it passes through the solution. Then a smaller volume with fewer nanoparticles would be sampled for the back part of the sample. Fewer nanoparticles exposed would lead to less absorption compared to the original beam, which would explain the increase of the bleach signal. Basically, due to the creation of the thermal lens inside the sample caused by strong laser excitation by the pump beam, more light will be transmitted, which is detected in the pump–probe experiments. Also, as the light is then collected behind the sample and focused into the entrance of a fiber optic cable, the small entrance area of the fiber optic cable can act as a pinhole. This geometric parameter could therefore contribute to a further increase in transmission for the sample.

The change in the measured signal is usually found to be proportional to the index gradient in the solution.<sup>21,22</sup> The thermal lensing effect is therefore enhanced in organic solvents and/or in surfactant solutions because their refractive indices are very sensitive to temperature changes.<sup>21,22</sup> As an example, the thermal lensing signal of excited 9-nitroanthracene in

isooctane is found<sup>22</sup> to be 41 times larger than in water. Hence, this effect should be further amplified in the presence of the AOT surfactant.<sup>21</sup>

In the case of metal particles in the size range of tens of nanometers and above, the temperature gradient generated around the particle can be large enough to be measured for individual particles.<sup>18,19</sup> A large number of photons are absorbed per particle due to the large absorption cross-section of the surface plasmon resonance. As the relaxation dynamics after laser excitation are essentially nonradiative, the absorbed photon energy is transferred into thermal lattice energy of the particle on the time scale of the electron–phonon coupling, giving rise to rapid lattice heating. The thermal equilibrium with the surrounding medium is then reached by a heat transfer between the particle lattice and its medium. For the silver nanodisks used in this study and considering the organic solvent and the presence of surfactants, the heat conductivity mismatch between the silver particles and the medium induces a large temperature gradient at the interface. As the medium refractive index depends on the temperature as  $dn/dT < 0$ , each particle behaves as a divergent lens with a similar behavior as the one described above.<sup>18</sup>

Taking into account that the signal is measured on an ensemble of particle, the role of the geometric interplay between the different lenses involved is not clear at this point. Nevertheless, the observed effect can be related to the intense heating of the nanoparticles environment. This thermal relaxation can be described by the following thermodynamic equation<sup>9,24</sup> for spherical particles:

$$T_2 = T_{2i} + \frac{k_1 R}{\Sigma r} (T_{2i} - T_{1i}) \left\{ \sqrt{\tau_1} \operatorname{erfc} \left( \frac{r-R}{2\sqrt{\alpha_2 t}} \right) - \frac{k_2 (\sqrt{\tau_1} + \sqrt{\tau_2})}{\Sigma \beta} \left[ \operatorname{erfc} \left( \frac{r-R}{2\sqrt{\alpha_2 t}} \right) - \exp \left( \frac{\beta(r-R)}{\sqrt{\alpha_2 t}} + \beta^2 t \right) \right] \operatorname{erfc} \left( \frac{r-R}{2\sqrt{\alpha_2 t}} + \beta \sqrt{t} \right) \right\}$$

where  $\Sigma = k_1 \sqrt{\tau_1} + k_2 \sqrt{\tau_2}$ ,  $\beta = (k_2 - k_1)/\Sigma$ ,  $\tau = R^2/\alpha$  is the relaxation time,  $\alpha = k/\rho c_p$  is the thermal diffusivity,  $k$  is the thermal conductivity,<sup>25</sup>  $T$  is the temperature,  $R$  is the particle radius, and  $r$  is the distance from the particle. Subscripts 1 and 2 denote the particle and the medium, respectively.  $T_{2i}$  and  $T_{1i}$  are the initial temperatures in each medium.

Calculations have been performed for a 20 nm particle and an initial electronic temperature variation  $\Delta T$  between 500 and 900 K as a function of the time and the distance from the nanoparticle surface. The relation between the temperature variation and the laser energy has been estimated taking into account the absorption of the silver nanodisk solution and its concentration. The silver concentration is measured using Lambert–Beer's law at 250 nm:  $\text{OD}_{250} = \epsilon_{250} l c$  where  $\epsilon_{250} = 16\,400$  L mol<sup>-1</sup> cm<sup>-1</sup> at  $\lambda = 250$  nm is the extinction coefficient,  $l = 0.2$  cm is the optical path length and  $\text{OD}_{250} = 0.6$  is the optical density in the present experiment. Hence the silver concentration is found to be  $C_{\text{Ag}} = 1.27 \times 10^{-9}$  mol L<sup>-1</sup> or  $C = 7.6 \times 10^{14}$  particles per liter (making use of the average particle size). Such a calculation is possible in the case of silver because the absorption in the UV range is due to interband transitions which do not depend on the particle size and shape. Assuming a focal volume of  $V_f = 10^{-7}$  L, the energy absorbed per particle,  $E_p$ , is estimated by  $E_p = E_t(1 - e^{-\text{OD}})/CV_f = 7.56 \times 10^{-9} E_t$ , where  $E_t$  is the laser energy. The temperature variation is then equal to  $\Delta T = E_p/mc_p = 1262 E_t$  with  $E_t$  in microjoules

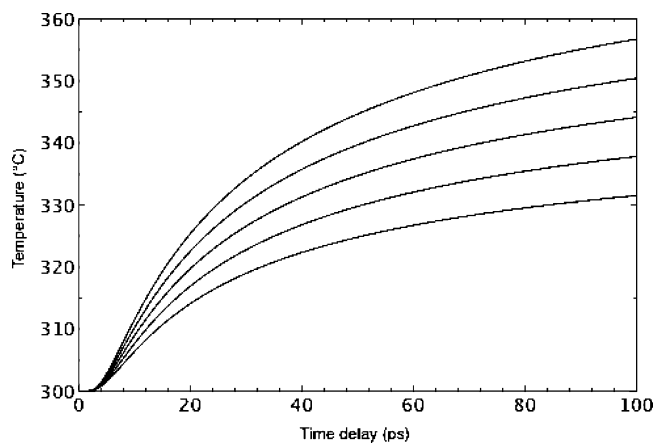


**Figure 4.** Variation of the temperature at a distance  $r = 100$  nm from a particle of diameter  $D = 2R = 20$  nm for different initial electron temperatures, between  $\Delta T = 500$  and  $900$  K. An exponential fit to the calculated temperature dependence shows that the temperature increases according to  $1 - e^{-t/\tau_2}$  with  $\tau_2 = 35$  ps in qualitative agreement with the experimental results.

where  $m = 2.58 \times 10^{-20}$  kg is the particle mass and  $c_p = 232$  J kg $^{-1}$  K $^{-1}$  is the specific heat capacity of silver. The distance from the surface has been chosen as  $r = 100$  nm because it corresponds to a sphere of diameter  $D = \lambda/2$ . For shorter distances, the temperature rise is more important but the characteristic size is below the diffraction limit. On the opposite, at longer distance, the temperature quickly decreases and contributes less to the signal.

Figure 4 represents the calculated temperature as a function of time for a 20 nm sphere, at a distance of 100 nm from the surface.

The initial temperatures are related to the experimental pump intensities as estimated above. The temperature increases exponentially and can be modeled by  $1 - e^{-t/\tau_2}$  with a time constant  $\tau_2 = 35$  ps, which is close to the experimental one  $\tau_2 = 40$  ps. In qualitative agreement with the experimental results, this time constant is found to be independent of the initial electronic temperature rise inside the nanoparticle.

The thermal lens effect (as well as a possible volume expansion) is most likely enhanced by the presence of spheres. The spheres absorb only above 450 nm but also contribute to the temperature increase of the solvent because they have a strong absorption at the wavelength of the pump pulse. This might explain why the short time signal, related to the disks only, is weaker than the long time one related to both shapes.

Because of the thermal lens created, the bleach does not depend on the probe wavelength and the plasmon resonance position. This is clearly observed in Figure 2B where the transient absorption spectrum exhibits a bleach proportional to the absorption. The rise time for the bleach at longer delay times therefore corresponds to the heat transfer between the hot metal nanoparticles and the surrounding medium, as observed through the thermal lens effect. The thermal lens is enhanced in the organic solvent in the presence of AOT surfactant. Further experiments are, however, necessary to elucidate the effect of

particle size and shape and the role of different solvents. Knowledge of the thermal relaxation in different solvents would help to understand the laser-induced shape transformations observed for metal nanoparticles.

## Conclusions

Silver nanodisks have been studied by static and ultrafast time-resolved pump-probe spectroscopy. The particles exhibit several surface plasmon resonances related to the particle shape. By time-resolved spectroscopy a large increase of the bleach intensity at long delay times ( $>20$  ps) after femtosecond laser excitation has been observed. This effect is likely to be due to a thermal lensing phenomenon induced by the fast heat transfer from the particle to its medium and a strong temperature dependence of the medium refractive index. This thermal lensing focuses the monitoring beam resulting in a decrease in the absorption (i.e., increase in the bleach) intensity.

**Acknowledgment.** We thank the support of the National Science Foundation (grant No. INT-0129263)—CNRS for an international cooperative grant.

## References and Notes

- (1) Jana, N. R.; Gearheart, L.; Murphy, C. J. *Langmuir* **2001**, *17*, 6782.
- (2) Yu, Y. Y.; Chang, S. S.; Lee, C. L.; Wang, C. R. C. *J. Phys. Chem. B* **1997**, *101*, 1588.
- (3) Ahmadi, T. S.; Wang, Z. L.; Henglein, A.; El-Sayed, M. A. *Chem. Mater.* **1996**, *8*, 1161.
- (4) Pinna, N.; Weiss, K.; Urban, J.; Pileni, M.-P. *Adv. Mater.* **2001**, *13*, 261.
- (5) Voisin, C.; Del Fatti, N.; Christofilos, D.; Vallee, F. *J. Phys. Chem. B* **2001**, *105*, 2264.
- (6) Hodak, J. H.; Martini, I.; Hartland, G. V. *J. Phys. Chem. B* **1998**, *102*, 6958.
- (7) Hodak, J. H.; Henglein, A.; Hartland, G. V. *J. Phys. Chem. B* **2000**, *104*, 9954.
- (8) Link, S.; El-Sayed, M. A. *Int. Rev. Phys. Chem.* **2000**, *19*, 409.
- (9) Hu, M.; Hartland, G. V. *J. Phys. Chem. B* **2002**, *106*, 7029.
- (10) Mohamed, M. B.; Ahmadi, T. S.; Link, S.; Braun, M.; El-Sayed, M. A. *Chem. Phys. Lett.* **2000**, *317*, 517.
- (11) Link, S.; Furube, A.; Mohamed, M. B.; Asahi, T.; Masuhara, H.; El-Sayed, M. A. *J. Phys. Chem. B* **2002**, *106*, 945.
- (12) Link, S.; Hathcock, D. J.; Nikoobakht, B.; El-Sayed, M. A. *Adv. Mater.* **2003**, *15*, 393.
- (13) Link, S.; Burda, C.; Nikoobakht, B.; El-Sayed, M. A. *J. Phys. Chem. B* **2000**, *104*, 6152.
- (14) Maillard, M.; Giorgio, S.; Pileni, M.-P. *Adv. Mater.* **2002**, *14*, 1084.
- (15) Maillard, M.; Giorgio, S.; Pileni, M.-P. *J. Phys. Chem. B* **2003**, *107*, 2466.
- (16) Tsuyumoto, I.; Sawada, T. *Bull. Chem. Soc. Jpn.* **2000**, *73*, 507.
- (17) Weimer, W. A.; Dovichi, N. *J. Appl. Phys.* **1986**, *59*, 225.
- (18) Mawatari, K.; Kitamori, T.; Sawada, T. *Anal. Chem.* **1998**, *70*, 5037.
- (19) Boyer, D.; Tamarat, P.; Maali, A.; Lounis, B.; Orrit, M. *Science* **2002**, *297*, 1160.
- (20) Petit, C.; Lixon, P.; Pileni, M. P. *J. Phys. Chem.* **1993**, *97*, 12974.
- (21) Tran, C. D.; Van Fleet, T. A. *Anal. Chem.* **1988**, *60*, 182.
- (22) Tran, C. D.; Van Fleet, T. A. *Anal. Chem.* **1988**, *60*, 2478.
- (23) Uchiyama, K.; Hibara, A.; Kimura, H.; Sawada, T.; Kitamori, T. *Jpn. J. Appl. Phys.* **2000**, *39*, 5316.
- (24) Cooper, F. *Int. J. Heat Mass Transfer* **1977**, 991.
- (25)  $\alpha_1 = 1.75 \times 10^{-4}$  m $^2$  s $^{-1}$ ,  $\alpha_2 = 6.71 \times 10^{-8}$  m $^2$  s $^{-1}$ ,  $k_1 = 428$  J s $^{-1}$  m $^{-1}$  K $^{-1}$ ,  $k_2 = 0.0967$  J s $^{-1}$  m $^{-1}$  K $^{-1}$ . Tabulated data taken from *CRC Handbook for silver* and: Riddick, J. A.; Bunger, W. B.; Sakano, T. K. In *Organic solvents, Physical properties and Methods of Purification*. Techniques of Chemistry; J. Wiley: New York, Chichester, Brisbane, 1986 (for the solvent).